ACS OMEGA

http://pubs.acs.org/journal/acsodf

Article

Highly Sensitive and Selective DNA Sequencing Device Using Metal Adatom Adsorption on 2D Phosphorene

Junfeng Zheng,[▽] Xuan Zhang,[▽] Youhao Yang, Jin Cui, Liang Fang, Miao Zhou, and Qian Chen*

Cite This: *ACS Omega* 2023, 8, 17768−17778

Read Online

ACCESS | Metrics & More | Article Recommendations | Supporting Information

ABSTRACT: Two-dimensional (2D) material revolutionarily extends the technique capability of traditional nanopore/nanogap-based DNA sequencing devices. However, challenges associated with DNA sequencing on nanopores still remained in improving the sensitivity and specificity. Herein, by first-principles calculation, we theoretically studied the potential of transition-metal elements (Cr, Fe, Co, Ni, and Au) anchored on monolayer black phosphorene (BP) to act as all-electronic DNA sequencing devices. The spin-polarized band structures appeared in Cr-, Fe-, Co-, and Au-doped BP. Remarkably, the adsorption energy of nucleobases can be significantly enhanced on BP with Co, Fe, and Cr doping, which contribute to the enlarged current signal and lower noise levels. Furthermore, the order of nucleobases in terms of their adsorption energies onto the Cr@BP is C > A > G > T, which exhibits more distinct adsorption energies than Fe@BP or Co@BP. Therefore, Cr-doped BP is more effective to avoid ambiguity in recognizing various bases. We thus envisaged a possibility of a highly sensitive and selective DNA sequencing device based on phosphorene.

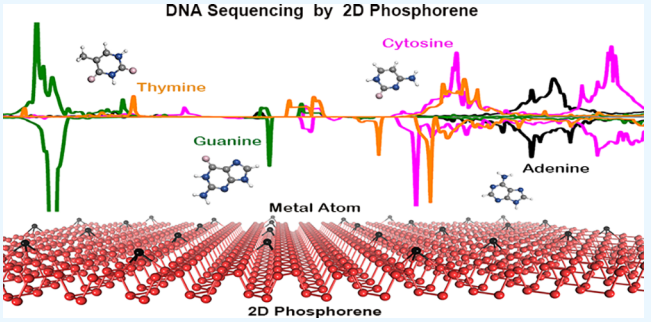

1. INTRODUCTION

DNA sequencing is a pivotal tool in rapidly expanding personal genomics where individual genomes are genotyped and bioinformatically analyzed to find disease association of genes and loci.[1] Meanwhile, fast, low-cost, and reliable methods for DNA sequencing are necessary prerequisites for the improvement of medical diagnosis and treatment.[2,3] Accordingly, ambitious programs have been introduced to drive the cost of genome sequencing down toward a much anticipated target.[4,5] Nanopore/nanogap-based DNA sequencing,[6,7] beyond established and well-developed chemical and enzymatic methods,[8,9] has long promised to provide cheaper, faster, and accurate DNA sequencing. However, sequencing still needs further improvement, especially in terms of quality and technology.

Extensive experimental studies on DNA in a solid-state nanopore have been carried out and provide a comprehensive understanding of nanopore DNA sequencing.[10−13] The past decade has witnessed a rapidly growing number of reports on two-dimensional (2D) material nanopore-based biosensing applications.[14−18] However, reading DNA sequences at a single-base resolution is still far from being achieved.[19] The development of the state of the art of graphene-based nanodevices is discussed in some of the recent review articles.[6,20] In 2011, Min and co-workers have theoretically demonstrated the feasibility of DNA sequencing using a fluidic nanochannel functionalized with a graphene nanoribbon.[21] Moreover, Prasongkit and co-workers have reported that solid nanopore-based techniques help to achieve a single-nucleotide or base resolution.[22] Computational realization of DNA detection through graphene-based nanochannels and nanopores has also been reported.[20,23]

A series of challenges, such as fast DNA translocation across the pores and high levels of current noise, hinder the development of this technique.[24,25] Phosphorene has been considered as a new alternative to graphene for the next-generation semiconductor-based devices.[26,27] Monolayer BP has received extensive attention due to its biocompatibility, low cytotoxicity, and unique optical, electronic, and mechanical properties.[28,29] Meanwhile, BP has a wide tunable band gap compared to graphene.[30] More importantly, it has been found that BP nanostructures are chemically and structurally stable in air and water,[31−33] meaning less hydrophobic than graphene. Hence, it has been considered as a promising competitor to graphene as for DNA sequencing.

In this paper, we theoretically study the potential of phosphorene decorated with transition-metal atoms (Cr, Fe, Co, Ni, and Au) to act as an all-electronic DNA sequencing device. The spin-polarized band structures appeared in Cr-, Fe-,

Received: January 26, 2023
Accepted: April 26, 2023
Published: May 10, 2023

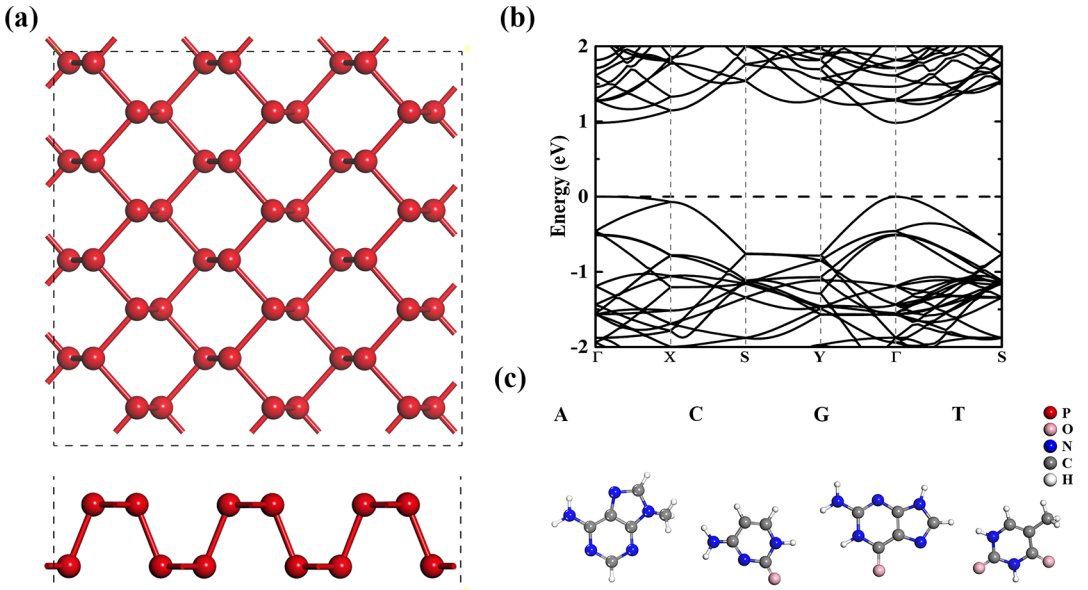

Figure 1. (a) Illustration of the top and side view of phosphorene. (b) Band structure of pristine phosphorene. (c) DNA nucleobases employed in the simulations: adenine (A), cytosine (C), guanine (G), and thymine (T).

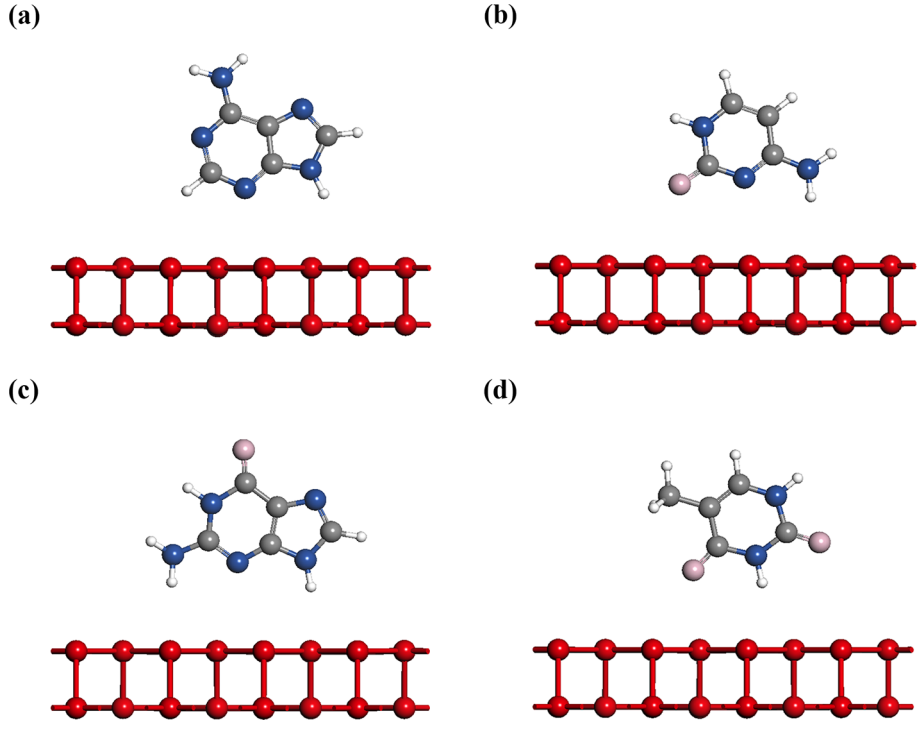

Figure 2. Optimized structure of different nucleobases' adsorption on pristine phosphorene. (a) Adenine adsorption on pristine phosphorene. (b) Cytosine adsorption on pristine phosphorene. (c) Guanine adsorption on pristine phosphorene. (d) Thymine adsorption on pristine phosphorene.

Co-, and Au-doped phosphorene. The adsorption energy of DNA nucleobases on BP can be significantly enhanced with the decoration of Co, Fe, and Cr. These results imply an enhanced current signal and lower noise levels. Our work provides beneficial directions and supports for DNA sequencing based on BP with excellent stability and adjustable electronic properties.

2. MODEL AND COMPUTATIONAL DETAILS

All first-principles calculations were performed within spin-polarized density functional theory (DFT) as implemented in the Vienna ab initio simulation package (VASP)[34,35] with the generalized gradient approximation (GGA) proposed by Perdew, Burke, and Ernzerhof (PBE).[36] Projector-augmented wave (PAW) potentials were employed to describe the ion−electron interaction.[37] We adopted the optPBE-vdW[38] functional to properly treat the effect of the van der Waals interaction between phosphorene and DNA nucleobases. The lattice constant of a fully optimized primitive unit cell is 3.35 × 4.62 Å, which has four P atoms arranged in an orthorhombic primitive unit cell. Figure 1a shows the top and side views of a 4 × 3 phosphorene supercell (containing 48 P atoms). Thus, the adatom−phosphorene systems correspond to a concentration of

https://doi.org/10.1021/acsomega.3c00540
ACS Omega 2023, 8, 17768−17778

2.08%. To avoid the artificial interaction with the neighboring unit cell, the supercell size of the scattering region was set to 13.4 × 13.86 Å. The energy cutoff was set to be 400 eV, and the Monkhorst−Pack *k*-grid mesh was 3 × 3 × 1 in surface calculations. The theoretical lattice was used by performing structural optimization until the force of each atom was less than 0.03 eV/Å. In the direction perpendicular to the phosphorene layer, we used a slab consisting of one bilayer separated from its periodic image perpendicular to the surface by a vacuum gap of 20 Å. Ab initio molecular dynamics simulation (AIMD) was performed for 5 ps with a time step of 1.0 fs at the temperature of 300 K to gauge the stability of the structure.

The adsorption energy (E_a) of different nucleobases on phosphorene was computed using the following equation:

$$E_a = E_{total} - (E_n + E_{sur}) \quad (1)$$

where E_{total} represents the total energy of the whole adsorption system. E_n and E_{sur} are the energies of isolated nucleobases and the clean substrate, respectively. By this definition, a larger negative value of E_a denotes a stronger interaction between the molecule and the surface.

3. RESULTS

To ensure that phosphorene is rendered correctly, we first calculated the band structure of the pristine layer. Figure 1a shows the top and side views of a 4 × 3 phosphorene supercell (containing 48 P atoms). Thus, the adatom−phosphorene systems correspond to a concentration of 2.08%. Phosphorene is a semiconductor with an orthogonal structure without magnetism.[39] The lattice of phosphorene is interconnected six membered rings, which has upper and lower layers, and each atom in the lattice is covalently bound to the other 3 atoms. The band structure of the pristine layer is shown in Figure 1b. Clearly, the phosphorene has a direct band gap of 1 eV. Meanwhile, the valence band maximum (VBM) and the conduction band minimum (CBM) are both located at the Γ point, which agree well with the previous theoretical study.[39] Figure 1c shows the molecular structure of four nucleobases: adenine (A), cytosine (C), guanine (G), and thymine (T).

We first calculated the adsorption of nucleobases on pristine phosphorene. Figure 2 shows the optimized structures of different nucleobases on pristine phosphorene. We found that nucleobase molecules were perpendicular to phosphorene. The detailed adsorption energies of nucleobases on pristine phosphorene are listed in Table 1. In addition, the adsorption distance from the basal plane to the nucleobase position is also presented. Here, we defined the adsorption distance as a difference between the lowest atom of the nucleobases and the average height of the three nearest P atoms. Adsorption energies for A, C, G, and T on pristine phosphorene are −0.4, −0.46, −0.43, and −0.39 eV, respectively. Correspondingly, adsorption distances for A, C, G, and T on pristine phosphorene are 3.06, 3.3, 2.65, and 2.53 Å, which indicates the physical adsorption.

Table 1. The Calculated Adsorption Energy (E_a) and Adsorption Distance (Å) of Nucleobases on Pristine BP

	adsorption energy E_a (eV)	distance (Å)
A	−0.40	3.06
C	−0.46	3.30
G	−0.43	2.65
T	−0.39	2.53

For pristine phosphorene, the subtle difference of adsorption energy makes these bases indistinguishable.

In order to further understand the difference in nucleobase adsorption on pristine phosphorene, we calculated the density of states of those adsorption systems. As shown in Figure 3, it can be clearly seen that in four nucleobases on pristine phosphorene, the band gap of 1 eV remains similar to the pristine phosphorene. Furthermore, nucleobase orbitals have no hybridization with phosphorene, leading to weak adsorption.

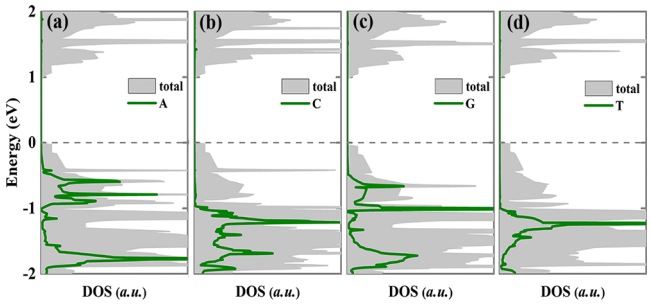

Figure 3. Total and projected density of states for different nucleobases on pristine phosphorene. (a) Total and projected density of states for adenine on pristine phosphorene. (b) Total and projected density of states for cytosine on pristine phosphorene. (c) Total and projected density of states for guanine on pristine phosphorene. (d) Total and projected density of states for thymine on pristine phosphorene.

Before studying the adsorption of nucleobases on metal-doped phosphorene, we examined the physical properties of the metal-doped systems. For BP, there are 3 adsorption sites (Figure 4): hollow (H), bridge (B), and on-top (T), whose different adsorption conditions have different stability. Present research has found that the H site is the most stable one for metal adsorption.[40] The adatoms (Co, Fe Cr, Ni, or Au) considered in this study preferred the hollow site of the hexagonal structure of phosphorene.[39] On this basis, we constructed the geometry. Figure 5 shows the band structures and DOS of monolayer BP with metal atoms adsorbing at the H site. Thus, by doping Cr, Fe, and Co on phosphorene, we introduced magnetism to systems. It is obvious that the magnetic moment stems from the 3d orbitals in Cr, Fe, and Co. For instance, Fe, which is a typical 3d transition-metal element, has an unfilled d orbital. Hence, with the adsorption of the Fe atom, impurity states and spin polarizations occurred in the systems. Furthermore, the value of the band gap reduces to 0.68 eV with the conduction and valence bands moving toward the Fermi energy level. In general, Au does not show a magnetic moment in its bulk counterpart. Interestingly, however, we found a magnetic moment in Au-

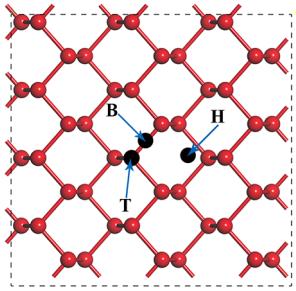

Figure 4. Illustration of the top view of BP and three adsorption sites. (H) Hollow site. (B) Bridge site. (T) On-top site.

https://doi.org/10.1021/acsomega.3c00540
ACS Omega 2023, 8, 17768−17778

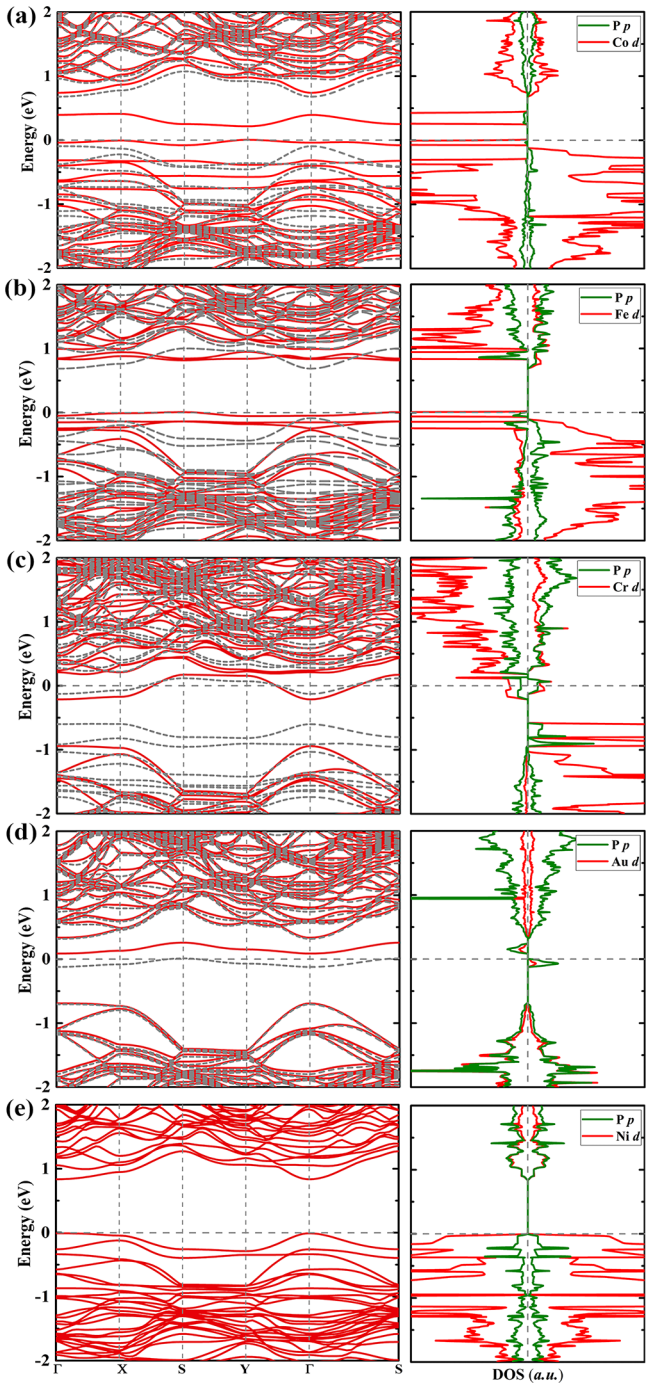

Figure 5. Calculated band structures and density of states (DOS) of adatom−BP systems. (a) Co, (b) Fe, (c) Cr, (d) Au, and (e) Ni.

doped systems. In contrast, there is no spin-polarized state in the Ni-doped case (Figure 5e). These results are similar to those that have been well-documented.[39] We also calculate metal clusters as previously described.[41] The optimized atomic structures of metal clusters adsorbed to BP are shown in Figure S1. The binding energy of 2-atom clusters to BP was smaller than that of 3-atom clusters. The binding energy of clusters adsorbed to the BP monolayer increases with the number of metal atoms. In addition, we performed analysis based on orbital projected DOS to reveal the bonding mechanism of metal clusters on the BP as shown in Figures S2 and S3.

Next, we studied the adsorption of nucleobases on phosphorene decorated with metal (Cr, Fe, Co, Ni, or Au) atoms (Figure 6). The distances between adsorbed molecules and underlying phosphorene and adsorption energies are listed in Table 2. It shows an increased adsorption and decreased adsorption distances on phosphorene decorated with metal adatoms compared to that on pristine phosphorene. Moreover, the adsorption for C is stronger than that for the other nucleobases (A, G, and T) on the decorated substrate, which is similar to the case in the pristine one. Especially for the Co adatom on phosphorene, the adsorption energies for A, C, G, and T on the system are −1.4, −1.42, −1.24, and −1.07 eV, respectively, which are roughly triple of that on the pristine phosphorene, indicating chemisorbed adsorptions rather than typical van der Waals interactions.

The largest adsorption energy, −1.42 eV, is found in the C adsorption system. However, the adsorption energy shows a barely noticeable difference between A and C adsorption systems. Moreover, the E_a for the G adsorption system is ∼0.18 eV, which is obviously lower than that in the C adsorption system. Correspondingly, adsorption distances for A, C, G, and T on pristine phosphorene are 1.98, 2.01, 2.02, and 1.95 Å, respectively, which are all smaller than that on the pristine one.

Interestingly, the adsorption energy of the Fe adatom on phosphorene follows the trend of the Co adatom on phosphorene. The adsorption energies for A, C, G, and T on the Fe adatom system are −1.35, −1.42, −1.29, and −1.16 eV, respectively. Similar to the adsorption of the Co adatom system, these still roughly triple that on the pristine phosphorene. For the Fe adatom system, the C adsorption system shows the largest adsorption energy. In addition, the adsorption average distance decreases from ∼2.8 Å on the Fe adatom system to 1.9 Å on pristine phosphorene. This also indicates the enhancement of molecular adsorption by the Fe adatom on phosphorene.

Meanwhile, in the Au-doped case, the adsorption energies for A, C, G, and T are −0.85, −0.98, −0.70, and −0.34 eV, respectively. On the whole, the adsorption energy was smaller than other cases, while the adsorption distance shows no significant difference compared to other cases. Moreover, the C adatom system still has a larger adsorption energy than other nucleobases. For the Ni-doped case, we found a similar conclusion with the Au-doped case.

For the Cr adatom system, it was found that the Cr adatom has significant effects on the adsorption energy. For instance, the adsorption average distance was reduced to ∼2 Å. As shown in Table 2, the order of the adsorbed nucleobases onto the system in terms of adsorption energy is C > A > G > T. The adsorption energy of C on the Cr adatom system increased from −0.42 eV on pristine BP to −1.56 eV on the Cr adatom system. Meanwhile, the adsorption energy increased from −0.40 to −0.95 eV for A, from −0.43 to −0.84 eV for G, and from −0.39 to −0.79 eV for T. The Cr adatom on phosphorene not only enhanced the adsorption energy but also gave rise to larger separation of the adsorption energies, which means unambiguous recognition of nucleobases over other metal adatom systems. In addition, ab initio molecular dynamics simulations[42] showed reasonable equilibration for the Cr adatom framework under 300 K (Figure S4), indicating its perfect thermal stability.

In order to understand the adsorption of different nucleobases on adatom-phosphorene systems, the electronic structures were further investigated. Figure 6a shows the partial DOS of different nucleobase adsorption systems. Clearly, the main contribution of the nucleobases' HOMO levels spans from −2.0 to 0 eV

https://doi.org/10.1021/acsomega.3c00540
ACS Omega 2023, 8, 17768−17778

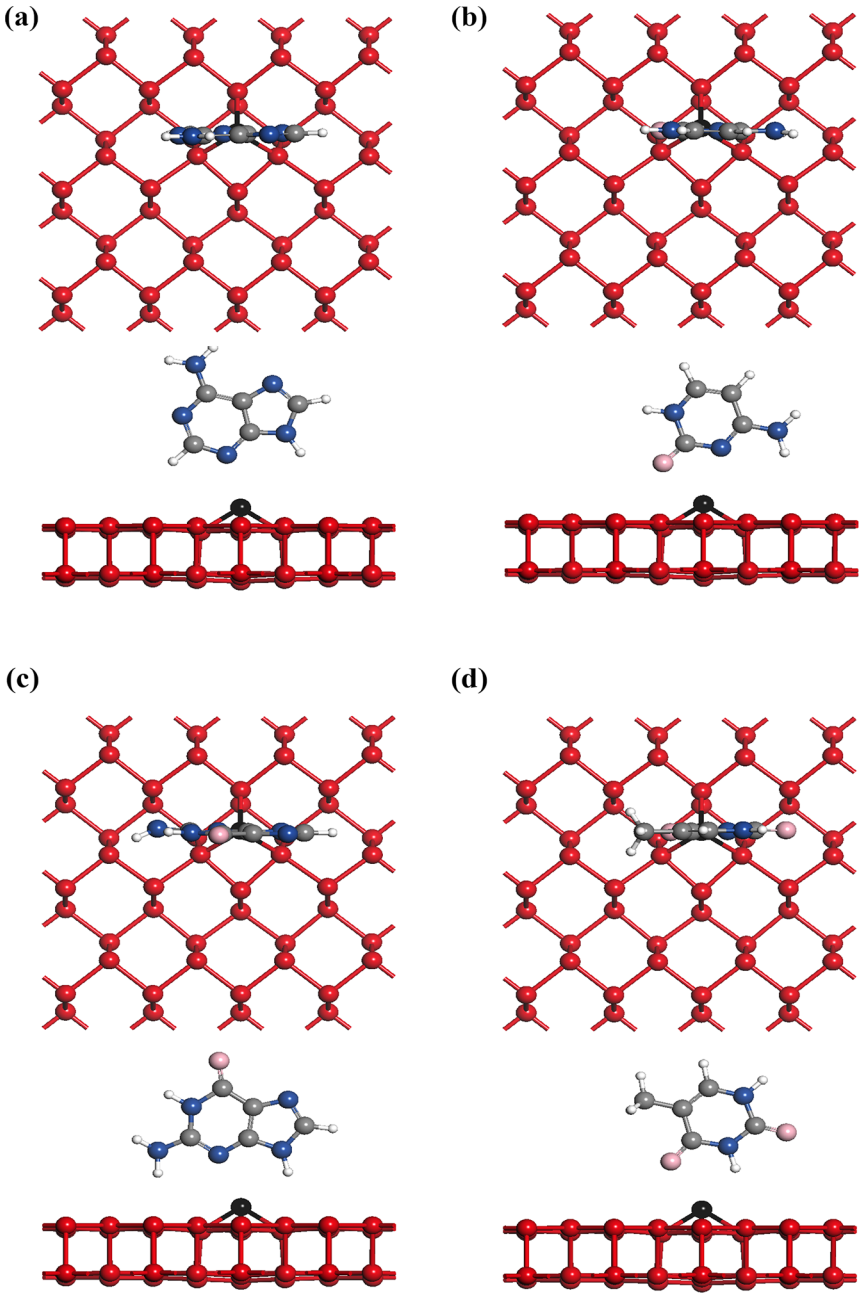

Figure 6. Optimized structures of nucleobases adsorbing on phosphorene with metals (Cr, Fe, Co, Ni, and Au) anchored at hollow sites. (a) Adenine. (b) Cytosine. (c) Guanine. (d) Thymine.

Table 2. Calculated Adsorption Distance (Å) and Adsorption Energy (E_a) of Different Nucleobases on Phosphorene with Metal Adsorption

	adsorption energy E_a (eV)					distance (Å)				
	BP-Co	BP-Fe	BP-Cr	BP-Au	BP-Ni	BP-Co	BP-Fe	BP-Cr	BP-Au	BP-Ni
A	−1.40	−1.35	−0.95	−0.85	−1.30	1.98	1.97	2.04	2.01	1.94
C	−1.42	−1.42	−1.56	−0.98	−1.36	2.01	1.95	1.94	1.99	1.98
G	−1.24	−1.29	−0.84	−0.70	−1.22	2.02	2.00	2.06	2.12	1.99
T	−1.07	−1.16	−0.79	−0.34	−0.93	1.95	1.92	1.90	2.22	1.93

below the Fermi level. This allows us to correlate the resonances in the transmission with the nucleobases' molecular states. For instance, the Co adatom-phosphorene systems containing adenine (A) present marked spin-up HOMO states around −0.4 eV, while for C, G, and T, the spin-down component (HOMO) shifts closer to the Fermi level. Also, HOMOs of C, G, and T overlap at the −0.2 eV. This analysis is in agreement with the adsorption energy calculations, for which the adsorption energy of A increases from −0.4 (on pristine phosphorene) to −1.4 eV (on Co@phosphorene). As a consequence, for the Co

https://doi.org/10.1021/acsomega.3c00540
ACS Omega 2023, 8, 17768−17778

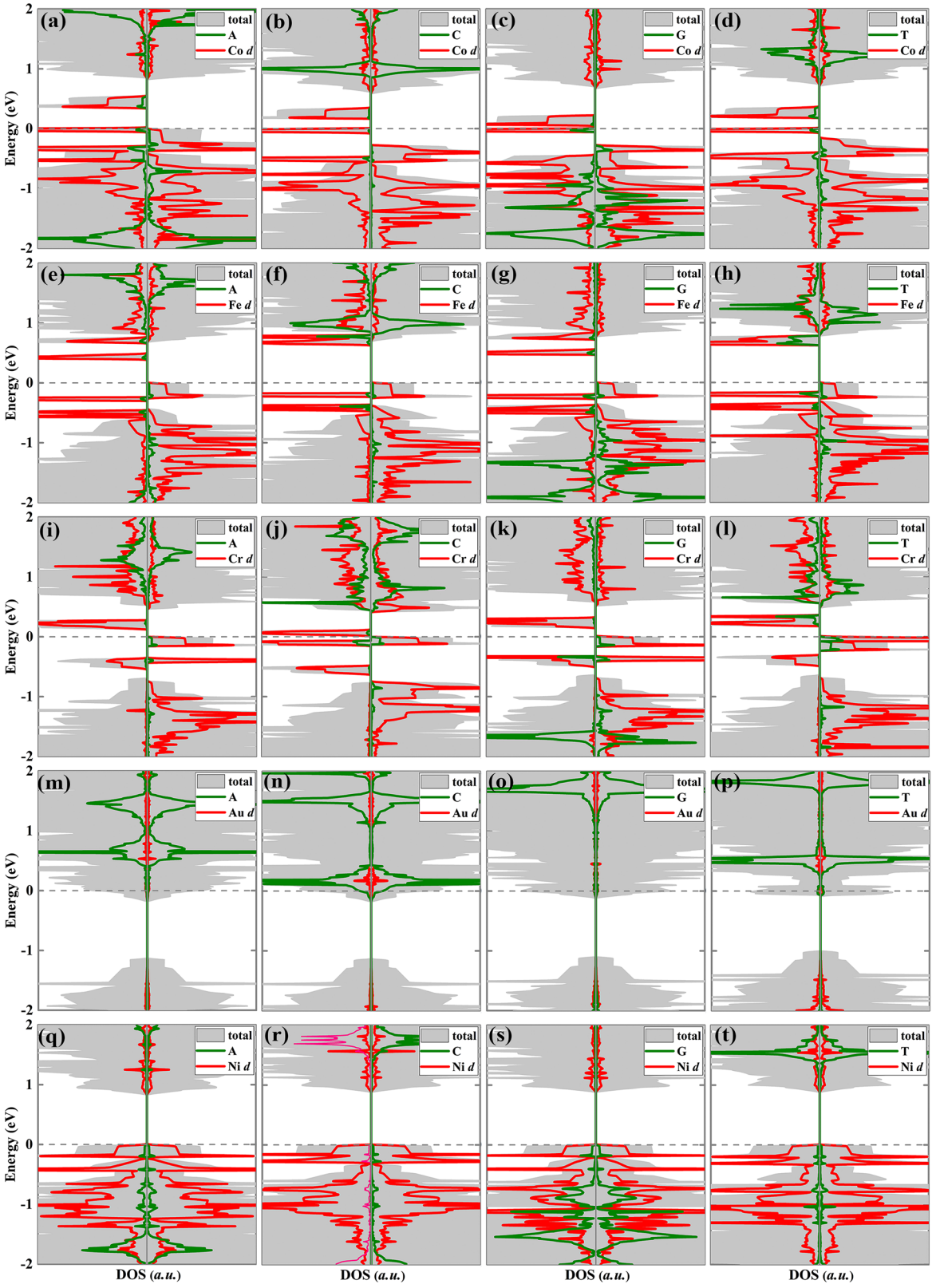

Figure 7. Calculated DOS of different nucleobases on phosphorene with metal adsorption. (a–d) Co-doped phosphorene. (e–h) Fe-doped phosphorene. (i–l) Cr-doped phosphorene. (m–p) Au-doped phosphorene. (q–t) Ni-doped phosphorene.

adatom-phosphorene system, a higher conductance difference should be found when A is located inside the system, while a difference between these three (C, G, and T) is slight. Therefore, Co adatom-phosphorene might not be a good device for DNA sequencing since it could not effectively distinguish the three nucleobases (C, G, and T).

The situation is little different for the adsorption of nucleobases on the Fe@phosphorene. As shown in Figure

https://doi.org/10.1021/acsomega.3c00540
ACS Omega 2023, 8, 17768−17778

7e−h, the Fe@phosphorene systems containing adenine (A) present marked spin-down HOMO states around −0.15 eV, while for C, G, and T, spin-down HOMO states are around −0.02, −0.13, and −0.23 eV, respectively.

For Cr@phosphorene systems, there were greater differences among different nucleobases. For instance, Figure 7i shows the partial DOS of A adsorption on Cr@phosphorene. Clearly, the A orbitals have an upshift. As such, the HOMO moves to the Fermi level, indicating that A loses electrons upon adsorption. With Cr adatoms on phosphorene, these orbitals of A become hybridized with the d states of the Cr atom, suggesting chemical bonding between A and the system. Similar effects can also be found in C, G, and T adsorption on Cr@phosphorene, which are shown in Figure 7j−l. Although there is overlap between nucleobase orbitals and electronic states of the Cr atom, it is actually easy to distinguish hybridization orbitals, suggesting the highly selective detection of nucleobases on Cr@phosphorene. For C adsorption on Cr@phosphorene, these orbitals become more delocalized and hybridized with the Cr d states, leading to enhanced adsorption. These results match with the adsorption energy calculations since the C has the largest adsorption energy. The charge density difference plot shows that the charge redistribution occurs around the entire structure of different nucleobases, and the shape of metal states can be easily identified. For the adsorption of different nucleobases, an enhancement of charge density redistribution can be observed at the interface when these nucleobases are absorbed on these systems (Figure 8), which is consistent with the hybridization of nucleobase orbitals and electronic states of the systems. Consequently, the adsorption energies were generally enhanced.

Lastly, the charge transfer between the adsorbed nucleobases and the substrate was qualitatively explored by the charge density difference and quantitatively by using Bader charge analysis. Figure 9A shows the charge density redistribution for A adsorption on Co@phosphorene. Clearly, charge redistribution spread almost over the molecule. For the adsorption of C, G, and T, similar charge transfer behaviors to that of A could be found. For A adsorption on metal@phosphorene, the Fe@phosphorene shows the most serious charge density redistribution, while the Cr@phosphorene shows the strongest change of charge density redistribution for C and G. For T adsorption on metal@phosphorene, the Co@phosphorene has the strongest change of charge density redistribution. For the Cr@phosphorene systems, it is obvious that the change of charge density redistribution was much stronger by comparing to the Co@phosphorene or Fe@phosphorene system. The physical origins lie in the major contribution of the electrostatic interaction in regulating the adsorption strength. As shown in Table 1, more charge transfer leads to higher adsorption energy. However, on the surface with metals, the adsorption strength is not only controlled by the electrostatic interaction but also by the direct hybridization between nucleobase orbitals and metal d states. However, Au or Ni showed weaker adsorption, which might also indicate the weaker charge transfer. Consequently, for Co, Fe, and Cr, the adsorption energies were generally enhanced, which is consistent with the hybridization of molecular orbitals and electronic states of the surface.

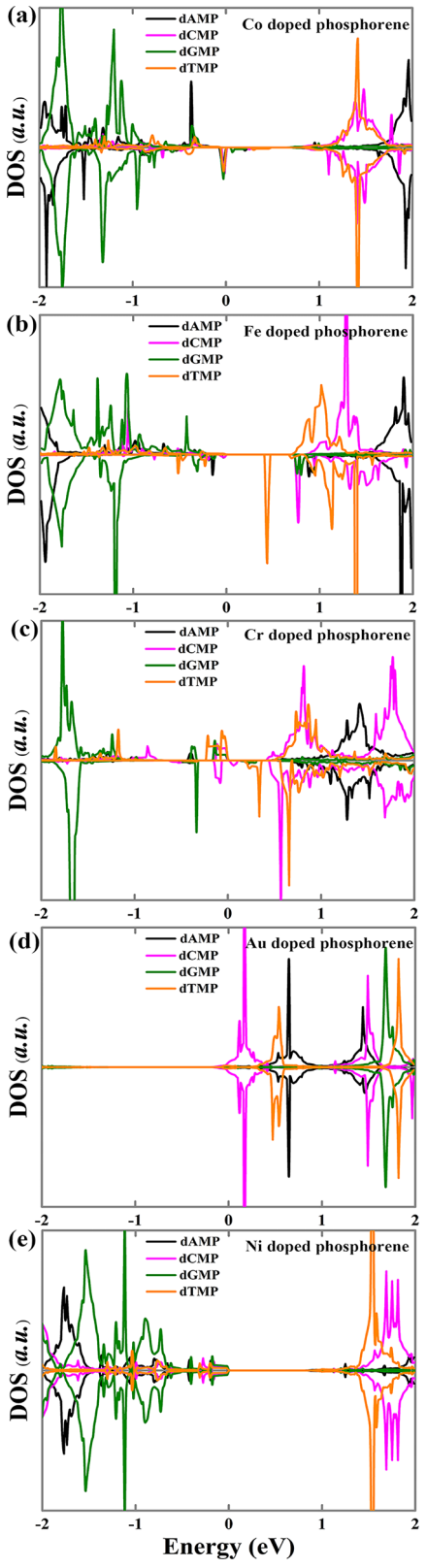

Figure 8. Charge density redistribution of different nucleobases on BP with metal adsorption. (a) Co-doped phosphorene. (b) Fe-doped phosphorene. (c) Cr-doped phosphorene. (d) Au-doped phosphorene. (e) Ni-doped phosphorene.

4. DISCUSSION

Here, we theoretically studied the potential of phosphorene decorated with transition-metal elements (Cr, Fe, Co, Ni, and Au) as all-electronic DNA sequencing devices by using DFT-based first-principles calculations. In some reports, graphene has to be sculpted into nanoribbons to acquire a band gap, which can measure resistive modulations to the transverse current due to DNA translocation through the pore.[23,43] BP, with an intrinsic

https://doi.org/10.1021/acsomega.3c00540
ACS Omega 2023, 8, 17768−17778

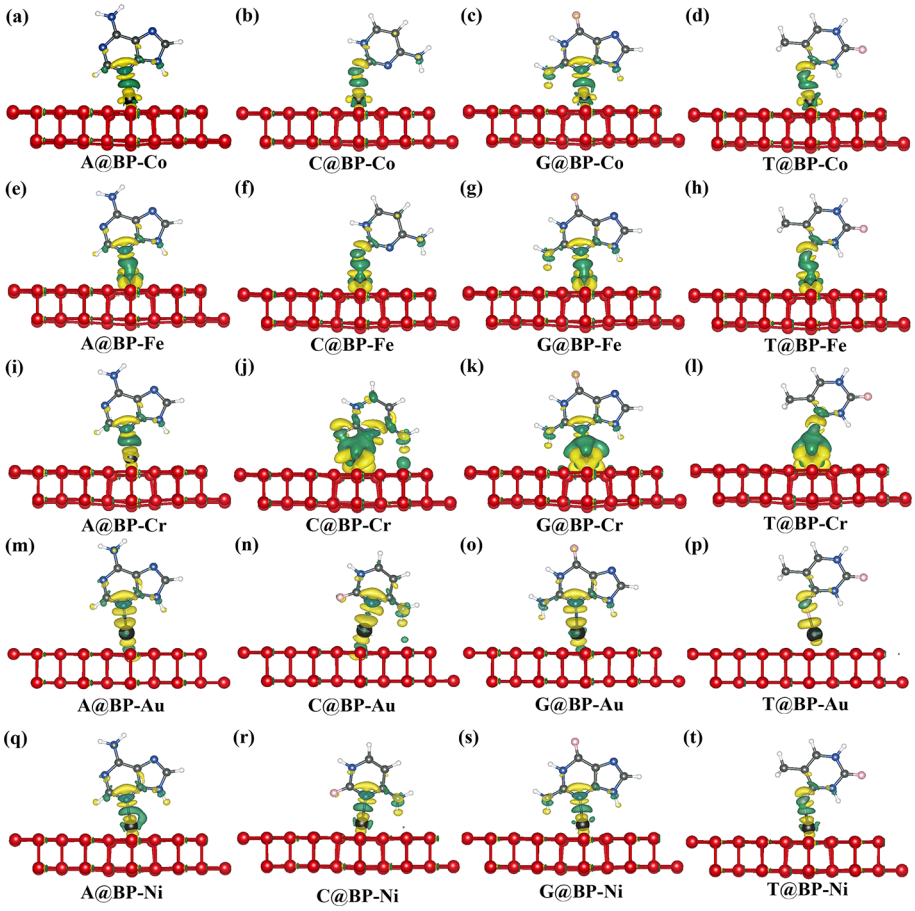

Figure 9. Calculated charge density redistribution for nucleobase adsorption on systems with an isovalue of 0.003 e/Å. The green color denotes electron accumulation, and the yellow color represents depletion. (a−d) Co-doped phosphorene. (e−h) Fe-doped phosphorene. (i−l) Cr-doped phosphorene. (m−p) Au-doped phosphorene. (q−t) Ni-doped phosphorene.

band gap, is therefore an attractive alternative for transverse current detection.[30] In 2017, Cupo and co-workers have theoretically and experimentally studied the BP nanoholes/nanopores with different radii.[44,45] A study has shown the potential biomedical applications of the phosphorene nanostructure as it does not affect the protein structures.[46] Therefore, we believe that these advances must facilitate the development of DNA sequencing techniques. Toward this goal, we first investigated the adsorption behaviors of nucleobases on pristine phosphorene. Our calculations showed that adsorption energies for A, C, G, and T on pristine phosphorene are −0.4, −0.46, −0.43, and −0.39 eV, respectively; thus, these subtle differences between adsorption energies make these bases hard to distinguish.

Most recently, it was found that the metal atom adsorption could extensively affect the charge carrier type and achieve the structural stability of BP with no damage to its pristine excellent properties.[47] Doping is a chemical means to amplify its electronic properties as the surface states can be effectively manipulated.[48] In addition, present research shows that doping specific metal atoms to 2D BP might lead to the physical characteristic changes of the whole system.[39] Cr, Fe, Co, and Au atom adsorptions on 2D phosphorene could even introduce magnetism into the system. In Cr-, Fe-, Co-, and Au-doped systems, researchers found a spin-polarized band structure.[39] The introduction of magnetism to material structure may make sense to the detection of nucleobase molecules. Inspired by all these reports, we thus proposed metal-decorated phosphorene-based nanodevices for DNA sequencing. Then, we showed that different nucleobases were attached onto phosphorene with metal (Cr, Fe, Co, Ni, or Au) adsorption. Remarkably, the adsorption energy of nucleobases can be significantly enhanced with Co, Fe, and Cr doping, which indicate an enhanced current signal and lower noise levels. Furthermore, the order of nucleobases in terms of their adsorption energy onto the Cr@BP is C > A > G > T. Thus, Cr doping is more effective to avoid ambiguity in recognizing various bases. The first four atoms (Cr, Fe, Co, and Ni) belong to typical 3d transition-metal elements. However, the spin-polarized band structures appeared in Cr-, Fe-, Co-, and Au-doped systems, except for adatom Ni. Within 3d transition metals, the adsorption energy became stronger and stronger with decreasing atomic radii, and the adsorption energy was generally larger than groups I−III metals, except for the Cr adatom.

However, minimization of the noise is a prerequisite for increasing the signal-to-noise ratio and the sensitivity of 2D material nanopores.[19] Under the practical conditions, many properties including surface roughness, surface charge densities, etc. could be dramatically different from each other, yielding a different translocation behavior of DNA.[49] Meanwhile, recent advances demonstrate that the thickness of the 2D membrane is a vital factor.[50,51] Park et al. showed that nanopores in multilayered h-BN membranes with a small exposed area could significantly reduce the current noise to a value

https://doi.org/10.1021/acsomega.3c00540
ACS Omega 2023, 8, 17768−17778

comparable to those in typical SiN_x nanopores to a few ways of increasing the mechanical stability of the 2D membrane.[52] Li et al. also reported that the electronic structure of few-layer phosphorene varies significantly with the number of layers, in good agreement with theoretical predictions.[53] Meanwhile, metal clusters adsorbed on phosphorene could increase the hybridization compared to the metal atom doping. Encouraged by these results, the DNA sensing performance of metal clusters adsorbed on phosphorene needs further investigation. These tests would also apply to the blue phosphorene, another 2D phosphorene form with a different exposed surface.[54] Next, it would be necessary to explore the surface properties of BP layers in controlling its sensing DNA performance in experiment.

5. CONCLUSIONS

Phosphorene might be one of the possible winners in the race toward the goal of single-base-resolution DNA sequencing. Our theoretical calculation would instruct future DNA sequencing experiments, providing beneficial directions and supports for DNA sequencing based on monolayer phosphorene with both stability and adjustable electronic properties. This work, together with recent progress in this field, could hopefully promote 2D material toward sequencing to match the commercial achievements of biological pores or even traditional solid-state nanopores. Hence, our study might be beneficial for the development of phosphorene-based nanodevices for DNA sequencing.

■ ASSOCIATED CONTENT

Supporting Information

The Supporting Information is available free of charge at https://pubs.acs.org/doi/10.1021/acsomega.3c00540.

Top and side views of the optimized atomic structure of metal clusters adsorbed to BP and calculated binding energies per cluster (Figure S1), calculated band structures and DOS of 2-metal-cluster BP systems (Figure S2), calculated band structures and DOS of 3-metal-cluster BP systems (Figure S3), and Cr adatom framework and the total energy after AIMD calculations under 300 K (Figure S4) (PDF)

■ AUTHOR INFORMATION

Corresponding Author

Qian Chen − *Biomedical Analysis Center, College of Basic Medicine, Army Medical University (Third Military Medical University), Chongqing 400038, P. R. China; Key Laboratory of Electromagnetic Radiation Protection, Ministry of Education, Army Medical University (Third Military Medical University), Chongqing 400038, China;* orcid.org/0009-0003-8190-8482; Email: hetoqc@tmmu.edu.cn

Authors

Junfeng Zheng − *Biomedical Analysis Center, College of Basic Medicine, Army Medical University (Third Military Medical University), Chongqing 400038, P. R. China*

Xuan Zhang − *Department of Pharmacology, College of Pharmacy and Laboratory Medicine, Army Medical University (Third Military Medical University), Chongqing 400038, P. R. China*

Youhao Yang − *Biomedical Analysis Center, College of Basic Medicine, Army Medical University (Third Military Medical University), Chongqing 400038, P. R. China*

Jin Cui − *United Microelectronics Center Co., Ltd. (CUMEC), Chongqing 401332, P. R. China*

Liang Fang − *Key Laboratory of Optoelectronic Technology & Systems (Ministry of Education), College of Optoelectronic Engineering, Chongqing University, Chongqing 400044, P. R. China*

Miao Zhou − *College of Physics, Chongqing University, Chongqing 400044, P. R. China*

Complete contact information is available at: https://pubs.acs.org/10.1021/acsomega.3c00540

Author Contributions

$^{\nabla}$J.Z. and X.Z. contributed equally to this work.

Notes

The authors declare no competing financial interest.

■ ACKNOWLEDGMENTS

This work is supported by the Natural Science Foundation of Chongqing (cstc2019jcyj-msxmX0408 and cstc2020jcyj-msxmX0686) and the Open Foundation of Key Laboratory of Electromagnetic Radiation Protection, Ministry of Education.

■ ABBREVIATIONS

A	adenine
BP	phosphorene
C	cytosine
CBM	conduction band minimum
DFT	density functional theory
E_a	adsorption energy
G	guanine
T	thymine
VBM	valence band maximum
2D	two-dimensional

■ REFERENCES

(1) Goldfeder, R. L.; Wall, D. P.; Khoury, M. J.; Ioannidis, J. P. A.; Ashley, E. A. Human genome sequencing at the population scale: a primer on high-throughput dna sequencing and analysis. *Am. J. Epidemiol.* **2017**, *186*, 1000−1009.

(2) Mardis, E. R. A decade's perspective on DNA sequencing technology. *Nature* **2011**, *470*, 198−203.

(3) Rabbani, B.; Tekin, M.; Mahdieh, N. The promise of whole-exome sequencing in medical genetics. *J. Hum. Genet.* **2014**, *59*, 5−15.

(4) Shendure, J.; Aiden, E. L. The expanding scope of DNA sequencing. *Nat. Biotechnol.* **2012**, *30*, 1084−1094.

(5) Hayden, E. C. Technology:The $1,000 genome. *Nature* **2014**, *507*, 294−295.

(6) Steinbock, L. J.; Radenovic, A. The emergence of nanopores in next-generation sequencing. *Nanotechnology* **2015**, *26*, No. 074003.

(7) Venkatesan, B. M.; Bashir, R. Nanopore sensors for nucleic acid analysis. *Nat. Nanotechnol.* **2011**, *6*, 615−624.

(8) Service, R. F. The race for the $1000 Genome. *Science* **2006**, *311*, 1544−1546.

(9) Collins, F. S.; Green, E. D.; Guttmacher, A. E.; Guyer, M. S.; on behalf of the US National Human Genome Research Institute. A vision for the future of genomics research. *Nature* **2003**, *422*, 835−847.

(10) Nef, C.; Pósa, L.; Makk, P.; Fu, W.; Halbritter, A.; Schönenberger, C.; Calame, M. High-yield fabrication of nm-size gaps in monolayer CVD graphene. *Nanoscale* **2014**, *6*, 7249−7254.

(11) Sadeghi, H.; Mol, J. A.; Lau, C. S.; Briggs, G. A.; Warner, J.; Lambert, C. J. Conductance enlargement in picoscale electroburnt graphene nanojunctions. *Proc. Natl. Acad. Sci.* **2015**, *112*, 2658−2663.

(12) Lau, C. S.; Mol, J. A.; Warner, J. H.; Briggs, G. A. D. Nanoscale control of graphene electrodes. *Phys. Chem. Chem. Phys.* **2014**, *16*, 20398−20401.

(13) Cao, Y.; Dong, S.; Liu, S.; He, L.; Gan, L.; Yu, X.; Steigerwald, M. L.; Wu, X.; Liu, Z.; Guo, X. Building high-throughput molecular junctions using indented graphene point contacts. *Angew. Chem., Int. Ed.* **2012**, *51*, 12228−12232.
(14) Liu, S.; Lu, B.; Zhao, Q.; Li, J.; Gao, T.; Chen, Y.; Zhang, Y.; Liu, Z.; Fan, Z.; Yang, F.; You, L.; Yu, D. Boron nitride nanopores: Highly sensitive DNA single-molecule detectors. *Adv. Mater.* **2013**, *25*, 4549−4554.
(15) Liu, K.; Lihter, M.; Sarathy, A.; Caneva, S.; Qiu, H.; Deiana, D.; Tileli, V.; Alexander, D. T. L.; Hofmann, S.; Dumcenco, D.; Kis, A.; Leburton, J.-P.; Radenovic, A. Geometrical effect in 2D nanopores. *Nano Lett.* **2017**, *17*, 4223−4230.
(16) Liu, K.; Feng, J.; Kis, A.; Radenovic, A. Atomically thin molybdenum disulfide nanopores with high sensitivity for DNA translocation. *ACS Nano* **2014**, *8*, 2504−2511.
(17) Danda, G.; Masih Das, P.; Chou, Y.-C.; Mlack, J. T.; Parkin, W. M.; Naylor, C. H.; Fujisawa, K.; Zhang, T.; Fulton, L. B.; Terrones, M.; Johnson, A. T. C.; Drndić, M. Monolayer WS2 nanopores for DNA translocation with light-adjustable sizes. *ACS Nano* **2017**, *11*, 1937−1945.
(18) Mojtabavi, M.; VahidMohammadi, A.; Liang, W.; Beidaghi, M.; Wanunu, M. Single-molecule sensing using nanopores in two-dimensional transition metal carbide (MXene) membranes. *ACS Nano* **2019**, *13*, 3042−3053.
(19) Qiu, H.; Zhou, W.; Guo, W. Nanopores in graphene and other 2D materials: A decade's journey toward sequencing. *ACS Nano* **2021**, 18848−18864.
(20) Heerema, S. J.; Dekker, C. Graphene nanodevices for DNA sequencing. *Nat. Nanotechnol.* **2016**, *11*, 127−136.
(21) Min, S. K.; Kim, W. Y.; Cho, Y.; Kim, K. S. Fast DNA sequencing with a graphene-based nanochannel device. *Nat. Nanotechnol.* **2011**, *6*, 162−165.
(22) Prasongkit, J.; Grigoriev, A.; Pathak, B.; Ahuja, R.; Scheicher, R. H. Transverse conductance of DNA nucleotides in a graphene nanogap from first principles. *Nano Lett.* **2011**, *11*, 1941−1945.
(23) Saha, K. K.; Drndić, M.; Nikolić, B. K. DNA base-specific modulation of microampere transverse edge currents through a metallic graphene nanoribbon with a nanopore. *Nano Lett.* **2012**, *12*, 50−55.
(24) Merchant, C. A.; Healy, K.; Wanunu, M.; Ray, V.; Peterman, N.; Bartel, J.; Fischbein, M. D.; Venta, K.; Luo, Z.; Johnson, A. T. C.; Drndić, M. DNA translocation through graphene nanopores. *Nano Lett.* **2010**, *10*, 2915−2921.
(25) Garaj, S.; Hubbard, W.; Reina, A.; Kong, J.; Branton, D.; Golovchenko, J. A. Graphene as a subnanometre trans-electrode membrane. *Nature* **2010**, *467*, 190−193.
(26) Lee, G.; Pearton, S. J.; Ren, F.; Kim, J. Two-dimensionally layered p-black phosphorus/n-MoS2/p-black phosphorus heterojunctions. *Acs Appl. Mater. Interfaces* **2018**, *10*, 10347−10352.
(27) Sorkin, V.; Cai, Y.; Ong, Z.; Zhang, G.; Zhang, Y. W. Recent advances in the study of phosphorene and its nanostructures. *Crit. Rev. Solid State Mater. Sci.* **2017**, *42*, 1−82.
(28) Castellanos-Gomez, A. Black Phosphorus: Narrow gap, wide applications. *J. Phys. Chem. Lett.* **2015**, *6*, 4280−4291.
(29) Kou, L.; Chen, C.; Smith, S. C. Phosphorene: Fabrication, properties, and applications. *J. Phys. Chem. Lett.* **2015**, *6*, 2794−2805.
(30) Pathak, B. Electronic transport through DNA nucleotides in atomically thin phosphorene electrodes for rapid DNA sequencing. *Acs Appl. Mater. Interfaces* **2019**, *11*, 219−225.
(31) Li, L.; Yu, Y.; Ye, G. J.; Ge, Q.; Ou, X.; Wu, H.; Feng, D.; Chen, X. H.; Zhang, Y. Black phosphorus field-effect transistors. *Nat. Nanotechnol.* **2014**, *9*, 372−377.
(32) Hanlon, D.; Backes, C.; Doherty, E.; Cucinotta, C. S.; Berner, N. C.; Boland, C.; Lee, K.; Harvey, A.; Lynch, P.; Gholamvand, Z.; Zhang, S.; Wang, K.; Moynihan, G.; Pokle, A.; Ramasse, Q. M.; McEvoy, N.; Blau, W. J.; Wang, J.; Abellan, G.; Hauke, F.; Hirsch, A.; Sanvito, S.; O'Regan, D. D.; Duesberg, G. S.; Nicolosi, V.; Coleman, J. N. Liquid exfoliation of solvent-stabilized few-layer black phosphorus for applications beyond electronics. *Nat. Commun.* **2015**, *6*, 8563.
(33) Yasaei, P.; Kumar, B.; Foroozan, T.; Wang, C.; Asadi, M.; Tuschel, D.; Indacochea, J. E.; Klie, R. F.; Salehi-Khojin, A. High-quality black phosphorus atomic layers by liquid-phase exfoliation. *Adv. Mater.* **2015**, *27*, 1887−1892.
(34) Kresse, G.; Furthmüller, J. Efficient iterative schemes for ab initio total-energy calculations using a plane-wave basis set. *Phys. Rev. B* **1996**, *54*, 11169−11186.
(35) Kresse, G.; Furthmüller, J. Efficiency of ab-initio total energy calculations for metals and semiconductors using a plane-wave basis set. *Comput. Mater. Sci.* **1996**, *6*, 15−50.
(36) Perdew, J. P.; Burke, K.; Ernzerhof, M. Generalized gradient approximation made simple. *Phys. Rev. Lett.* **1966**, *77*, 3865−3868.
(37) Blöchl, P. E. Projector augmented-wave method. *Phys. Rev. B* **1994**, *50*, 17953−17979.
(38) Klimeš, J.; Bowler, D. R.; Michaelides, A. Van der waals density functionals applied to solids. *Phys. Rev. B* **2011**, *83*, No. 195131.
(39) Hu, T.; Hong, J. First-principles study of metal adatom adsorption on black phosphorene. *J. Phys. Chem. C* **2015**, *119*, 8199−8207.
(40) Liu, H.; Neal, A. T.; Zhu, Z.; Luo, Z.; Xu, X.; Tománek, D.; Ye, P. D. Phosphorene: An unexplored 2D semiconductor with a high hole mobility. *ACS Nano* **2014**, *8*, 4033−4041.
(41) Mananghaya, M. R.; Santos, G. N.; Yu, D. Small transition metal cluster adsorbed on graphene and graphene nanoribbons: A density functional based tight binding molecular dynamics study. *Org. Electron.* **2018**, *63*, 355−361.
(42) Teshome, T.; Datta, A. Two-dimensional graphene−gold interfaces serve as robust templates for dielectric capacitors. *ACS Appl. Mater. Interfaces* **2017**, *9*, 34213−34220.
(43) Nelson, T.; Zhang, B.; Prezhdo, O. V. Detection of nucleic acids with graphene nanopores: ab initio characterization of a novel sequencing device. *Nano Lett.* **2010**, *10*, 3237.
(44) Pei, J.; Gai, X.; Yang, J.; Wang, X.; Yu, Z.; Choi, D.-Y.; Luther-Davies, B.; Lu, Y. Producing air-stable monolayers of phosphorene and their defect engineering. *Nat. Commun.* **2016**, *7*, 10450.
(45) Cupo, A.; Masih Das, P.; Chien, C. C.; Danda, G.; Kharche, N.; Tristant, D.; Drndić, M.; Meunier, V. Periodic arrays of phosphorene nanopores as antidot lattices with tunable properties. *ACS Nano* **2017**, *11*, 7494−7507.
(46) Cortés-Arriagada, D. Phosphorene as a template material for physisorption of DNA/RNA nucleobases and resembling of base pairs: A cluster DFT study and comparisons with graphene. *J. Phys. Chem. C* **2018**, *122*, 4870−4880.
(47) Feng, X.; Kulish, V. V.; Wu, P.; Liu, X.; Ang, K. W. Anomalously enhanced thermal stability of phosphorene via metal adatom doping: An experimental and first-principles study. *Nano Res.* **2016**, *9*, 2687−2695.
(48) Chowdhury, C.; Datta, A. Exotic physics and chemistry of two-dimensional phosphorus: phosphorene. *J. Phys. Chem. Lett.* **2017**, *8*, 2909−2916.
(49) Liang, L.; Shen, J.-W.; Zhang, Z.; Wang, Q. DNA sequencing by two-dimensional materials: As theoretical modeling meets experiments. *Biosens. Bioelectron.* **2017**, *89*, 280−292.
(50) Heerema, S. J.; Schneider, G. F.; Rozemuller, M.; Vicarelli, L.; Zandbergen, H. W.; Dekker, C. 1/f noise in graphene nanopores. *Nanotechnology* **2015**, *26*, No. 074001.
(51) Kumar, A.; Park, K. B.; Kim, H. M.; Kim, K. B. Noise and its reduction in graphene based nanopore devices. *Nanotechnology* **2013**, *24*, No. 495503.
(52) Park, K.-B.; Kim, H.-J.; Kim, H.-M.; Han, S. A.; Lee, K. H.; Kim, S.-W.; Kim, K.-B. Noise and sensitivity characteristics of solid-state nanopores with a boron nitride 2-D membrane on a pyrex substrate. *Nanoscale* **2016**, *8*, 5755−5763.
(53) Li, L.; Kim, J.; Jin, C.; Ye, G. J.; Qiu, D. Y.; da Jornada, F. H.; Shi, Z.; Chen, L.; Zhang, Z.; Yang, F.; Watanabe, K.; Taniguchi, T.; Ren, W.; Louie, S. G.; Chen, X. H.; Zhang, Y.; Wang, F. Direct observation of the layer-dependent electronic structure in phosphorene. *Nat. Nanotechnol.* **2017**, *12*, 21−25.

https://doi.org/10.1021/acsomega.3c00540
ACS Omega 2023, 8, 17768−17778

(54) Mukhopadhyay, T. K.; Datta, A. Ordering and dynamics for the formation of two-dimensional molecular crystals on black phosphorene. *J. Phys. Chem. C* **2017**, *121*, 10210−10223.

https://doi.org/10.1021/acsomega.3c00540
ACS Omega 2023, 8, 17768−17778